J Mater Sci (2009) 44:6717–6726
DOI 10.1007/s10853-009-3583-8

MESOSTRUCTURED MATERIALS

Hierarchical meso–macroporous titania-supported CuO nanocatalysts: preparation, characterization and catalytic CO oxidation

Jian-Liang Cao · Gao-Song Shao · Tian-Yi Ma · Yan Wang · Tie-Zhen Ren · Shi-Hua Wu · Zhong-Yong Yuan

Received: 30 November 2008 / Accepted: 12 May 2009 / Published online: 28 May 2009

Abstract Hierarchically mesoporous–macroporous titanium dioxide (MMTD) was synthesized by the hydrolysis of tetrabutyl titanate in the absence of surfactant and autoclaving at 60 °C, which exhibits a porous hierarchy of wormhole-like mesostructure in the framework of macrochannels. Different contents of CuO nanoparticles were supported on the MMTD by a deposition–precipitation (DP) method, retaining the high surface areas and hierarchical porosity. The prepared MMTD support and the resulting CuO/MMTD nanocatalysts were characterized by X-ray diffraction (XRD), scanning electron microscopy (SEM), transmission electron microscopy (TEM), N_2 adsorption analysis, temperature-programmed reduction (TPR), and X-ray photoelectron spectroscopy (XPS) techniques. Their catalytic behavior for low-temperature CO oxidation was studied by using a microreactor–GC system, and the CuO/MMTD catalyst with 8 wt% CuO content and calcined at 400 °C was found to have the highest catalytic activity. The catalytic activity depended on the CuO loading amount, the precalcination temperature, the meso–macroporous framework, the surface area, and the particle size of the CuO/MMTD catalysts.

J.-L. Cao · G.-S. Shao · T.-Y. Ma · Y. Wang · S.-H. Wu · Z.-Y. Yuan (✉)
Tianjin Key Laboratory of Energy-Material Chemistry (Tianjin) and Engineering Research Center of Energy Storage and Conversion (Ministry of Education), College of Chemistry, Nankai University, Tianjin 300071, People's Republic of China
e-mail: zyyuan@nankai.edu.cn

T.-Z. Ren
School of Chemical Engineering and Technology, Hebei University of Technology, Tianjin 300130, People's Republic of China

Introduction

Carbon monoxide, which is usually emitted from many industrial processes, transportation, chemical, agriculture, and domestic activities, is a strongly toxic gas and harmful to human health and environment. It is always one of the central issues in the environmental protection field. Catalytic oxidation of carbon monoxide is an efficient way to control the toxic emission. Although noble metal catalysts are very effective for catalytic oxidation of CO at low temperature [1–3], the base metal catalysts have deserved increasing attention due to their significant activity and lower cost. Supported-copper oxide catalysts, such as CuO/CeO_2 [4–6], CuO/TiO_2 [7, 8], CuO/Al_2O_3 [9, 10], $CuO/Ce_xZr_{1-x}O_2$ [11], $CuO/Ce_xSn_{1-x}O_2$ [6, 12], and CuO/Fe_2O_3 [13], have been found to be the potential alternatives for the catalytic oxidation of CO. The nature of the support is of crucial importance to the good catalytic performance of the resultant catalysts. Our recent studies have demonstrated that the high surface area and uniform mesoporosity of the oxide supports would give rise to well-dispersed and stable CuO-based catalyst nanoparticles on the surface upon calcination and reduction and, as a consequence, would show an improved catalytic performance [14, 15].

Recently, mesoporous metal oxide materials with macroporous structures have attractedmuch interest, because their structural features promise uses as potential supports and catalysts in heterogeneous catalysis for bulkier molecules where efficient diffusion of reactant molecules could be facilitated [16]. It has been demonstrated that hierarchical materials containing both interconnected macroporous and mesoporous structures have enhanced properties compared with single-sized pore materials due to increased mass transport through the material and maintenance of a specific surface area on the level of fine pore systems [16].

Mesoporous–macroporous metal oxides prepared by surfactant-assisted spontaneous assembly [17] were used as supports for Pd catalysts, and they were found to be powerful catalysts for total oxidation of toluene and chlorobenzene, among which Pd/TiO_2 presented the highest catalytic potential [18]. The meso–macroporous Pd-loaded ceria–zirconia catalysts exhibited higher catalytic activity for CO oxidation than the catalysts without macrochannel structures and the one prepared by the co-precipitation method [19]. In this study, we describe the synthesis of mesoporous titania materials with a macrochannel structure by a simple surfactant-free process, and their use as catalyst support of CuO nanoparticles. The resultant nanocatalysts showed high catalytic activity on low-temperature carbon monoxide oxidation. The influence of the CuO loading amount and the calcination temperature on the catalytic performance of the hierarchical meso–macroporous titania-supported CuO nanocatalysts were investigated in detail.

Experimental

Synthesis of meso–macroporous titania support

All the chemicals were used as received without further purification. Tetrabutyl titanate (Kermel, AR) was used as a precursor for the preparation of hierarchical meso–macroporous titanium dioxide (MMTD) powders. In a typical synthesis, 10 mL of tetrabutyl titanate was added dropwise into 100 mL of sulfuric acid solution (pH 2) under very slow stirring at room temperature until the titanium *n*-alkoxide hydrolyzed completely. The mixture was transferred into a Teflon-lined autoclave and heated statically at 60 °C for 2 days. The solid was then collected, washed with distilled water, and dried at 60 °C.

Preparation of supported CuO nanocatalysts

The supported catalysts, CuO/MMTD, were prepared by the deposition–precipitation (DP) method. At room temperature, 1 g of MMTD powders were first suspended in the aqueous solution of an appropriate amount of $Cu(NO_3)_2 \cdot 3H_2O$, and then, 0.25 mol/L of Na_2CO_3 solution was gradually added into the above suspended solution until the pH value of the mixed solution reached 9.0. After stirring for 1 h, the mixture was filtered and washed with distilled water. The obtained solid was dried at 80 °C for 4 h and subsequently calcined at 400 °C for 3 h, denoted as *x*%-CuO/MMTD, where *x* represents the percent weight content of CuO loaded. In order to make clear the influence of the calcination temperature on the catalyst property, a series of 8%-CuO/MMTD catalysts calcined at different temperature were prepared in the similar manner.

Sample characterization

X-ray diffraction (XRD) measurement was performed on a Rigaku D/max-2500 diffractometer with Cu Kα radiation at 40 kV and 100 mA in a scanning range of 3–80° (2θ). The diffraction peaks of the crystalline phase were compared with those of standard compounds reported in the JCPDS Date File. The average crystallite size was calculated from the peak width using the Scherrer's equation.

Scanning electron microscopy (SEM) was performed on a Shimadzu SS-550 microscope at 15 keV and a Philips XL30W/TMP microscope at 25 keV. Transmission electron microscopy (TEM) analysis was performed on a Philips Tecnai-G20 microscope, operating at 200 kV. The sample powders for TEM observation were dispersed in ethanol and treated with ultrasound for 5 min, and then deposited on a copper grid coated with preformed holey carbon film.

N_2 adsorption–desorption isotherms were collected at liquid nitrogen temperature using a Quantachrome NOVA 2000e sorption analyzer. The specific surface areas (S_{BET}) of the samples were calculated following the multi-point BET (Brunauer–Emmett–Teller) procedure. The pore-size distributions were determined from the adsorption branch of the isotherms using the BJH (Barett–Joyner–Halenda) method. Before carrying out the measurement, each sample was degassed at 200 °C for more than 6 h.

X-ray photoelectron spectroscopy (XPS) measurements were carried out on a Perkin-Elmer PHI 5600 spectrophotometer with the Mg Kα radiation. The operating conditions were kept constantly at 187.5 eV and 250.0 W. In order to subtract the surface charging effect, the C 1s peak has been fixed at a binding energy of 284.6 eV.

Temperature-programmed reduction (TPR) experiments were performed under the mixture of 5% H_2 in N_2 flowing (30 mL/min) over 50 mg of catalyst at a heating rate of 10 °C/min. The uptake amount during the reduction was measured by using a thermal conductivity detector (TCD). For comparison, H_2-TPR measurement of pure CuO was carried out over 4.7 mg of CuO powder.

Measurements of catalytic performance

Catalytic activity tests were performed using a continuous-flow fixed-bed microreactor. A stainless steel tube with an inner diameter of 16 mm was chosen as the reactor tube. About 200 mg catalyst power was placed into the tube. The reactant gas mixture consisting of 10 vol% CO and air for balance was passed through the catalyst bed with a typical space velocity (SV) of 11000 mL/h/g. No pretreatment was applied before the catalytic activity test. After reacted at one temperature for 30 min, quantitative analysis of CO was performed online by using a GC-509A gas

chromatograph equipped with a thermal conductivity detector (TCD). The activity was expressed by the conversion of CO.

Results and discussion

Catalyst characterization

XRD analysis

The hierarchically meso–macroporous titanium dioxide (MMTD) was prepared by the hydrolysis of tetrabutyl titanate in diluted sulfuric acid solution and the subsequent autoclaving, and the CuO/MMTD catalyst was obtained by the DP method. Figure 1 shows the X-ray diffraction (XRD) patterns of the as-synthesized MMTD support and 400 °C-calcined CuO/MMTD catalysts with different CuO loading amounts. It is seen that a bicrystalline structure (anatase and brookite) appeared in the as-synthesized MMTD, and the diffraction intensity of anatase phase enhanced after 400 °C-calcination. Such a bicrystalline structure retained in the CuO/MMTD catalysts; however, the diffraction intensity decreased slightly with the increase of the CuO loading. Correspondingly, the average crystallite sizes of the titanias, calculated by the Scherrer's formula, decreased with the loading of CuO (Table 1). Idakiev et al. [20] reported that in the mesoporous zirconia-supported gold catalyst system, due to the possible interaction between ZrO_2 and gold particles, the deposition of gold in higher content could restrain to a certain extent the crystallization of tetragonal ZrO_2 phase and the enlargement of gold particle size. In the present CuO/MMTD catalysts, the deposition of CuO on the MMTD support

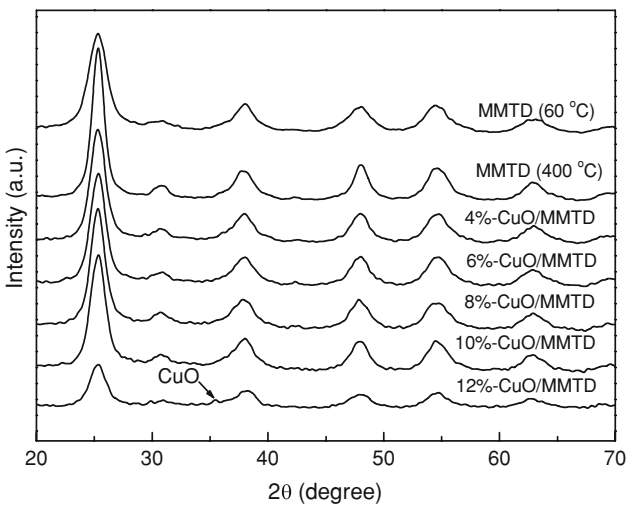

Fig. 1 XRD patterns of MMTD support and CuO/MMTD catalysts with different CuO loading amount calcined at 400 °C for 3 h

Table 1 Comparison of particle sizes, textural properties, and catalytic activities for CO oxidation of MMTD and CuO/MMTD catalysts

Catalysts	Calcination temperature (°C)	Mean particle size of MMTD (nm)	Mean particle size of CuO (nm)	Surface area[a] (m^2/g)	Pore volume[b] (cm^3/g)	$D_{BJH\text{-}ads}$[c] (nm)	Average pore diameter[d] (nm)	CO conversion (T/°C)
MMTD	60	6.2	–	266	0.235	2.6	3.5	–
MMTD	400	9.6	–	154	0.225	6.4	5.8	30.3% (240 °C)
4%-CuO/MMTD	400	8.5	–	178	0.253	5.6	5.7	100% (160 °C)
6%-CuO/MMTD	400	8.3	–	181	0.266	5.7	5.9	100% (150 °C)
8%-CuO/MMTD	400	7.9	–	158	0.227	5.9	5.8	100% (110 °C)
10%-CuO/MMTD	400	7.9	–	156	0.225	5.9	5.8	100% (140 °C)
12%-CuO/MMTD	400	7.5	14.5	154	0.195	4.6	5.1	100% (150 °C)
8%-CuO/MMTD	200	6.7	–	234	0.241	3.3	4.1	100% (125 °C)
8%-CuO/MMTD	300	7.0	–	201	0.243	4.5	4.8	100% (120 °C)
8%-CuO/MMTD	500	16.5	–	86	0.192	2.1, 10.8	9.0	100% (145 °C)
8%-CuO/MMTD	600	28.7	17.2	20	0.076	2.3, 22.7	15.3	100% (270 °C)

[a] Multi-point BET surface area

[b] Total pore volume at $P/P_0 = 0.99$

[c] Maximum of BJH pore diameter as determined from the adsorption branch

[d] Average pore diameter (4 V/A)

might also render the restraint effect on the crystallization of titania, indicating the possible interaction between the nanosized CuO particles and the MMTD support. When the CuO content was lower than 10 wt%, the corresponding CuO/MMTD catalysts did not show reflections characteristic of CuO structure. This may be due to the high dispersion of the CuO nanoparticles on the surface of the support and the CuO nanoparticles with particle sizes too small to be identified by the conventional X-ray diffraction method. Only when the CuO content increased to 12 wt%, the weak diffraction peaks attributed to CuO crystal phase appeared at 35.5° and 38.7° of 2θ, accompanied by the significant reduction of the diffraction intensity of titania. The average size of CuO particles in the 400 °C-calcined 12%-CuO/MMTD catalyst, calculated from the CuO (111) reflection peak at 38.7° of 2θ by the Scherrer formula, is 14.5 nm.

Figure 2 displays the XRD patterns of the 8%-CuO/MMTD catalysts calcined at different temperatures. With the increase of the calcination temperature, the diffraction peaks of the MMTD support were sharpened, indicating that the crystallization process went deeper. From 200 to 600 °C of the precalcination temperature of the CuO/MMTD catalysts, a progressive increase in the relative intensity of the lines of the anatase phase of MMTD support is seen, indicating an increase of the degree of crystallinity and the particle size of MMTD support by the thermal treatment. The brookite phase of titania disappeared and the rutile phase appeared after 600 °C-calcination, due to the occurrence of the crystalline phase transformation. Moreover, two weak diffractions at 35.5° and 38.7° (2θ), characteristic of CuO structure, were observed in the 600 °C-calcined catalysts, suggesting the growth of the CuO nanoparticles after high-temperature calcination of the catalyst system. The calculated particle sizes of titania supports and CuO catalysts are listed in Table 1.

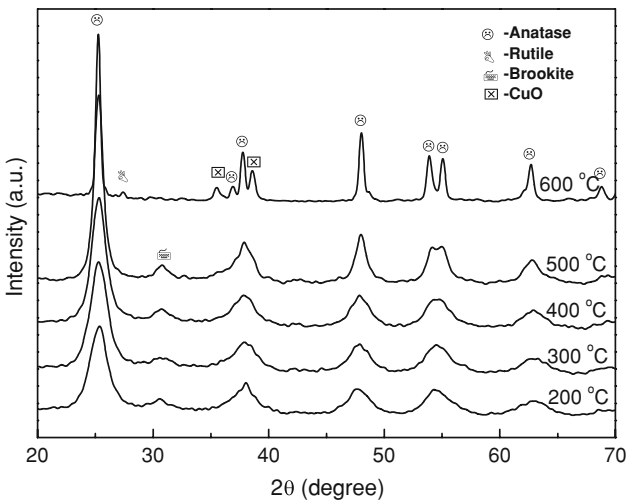

Fig. 2 XRD patterns of 8%-CuO/MMTD catalysts calcined at different temperatures

Electron microscopy

The hierarchical porous structure of the prepared MMTD samples and the CuO/MMTD catalysts are clearly observed in the electron microscopic images (Figs. 3 and 4). Figure 3a shows the typical scanning electron microscopy (SEM) images of the as-synthesized MMTD sample, presenting the channel-like macroporous structure with pore sizes in the range of 1–2.1 μm. The macrochannels are mainly of one-dimensional orientation, parallel to each other, perpendicular to the tangent of the surface of the particles. A close observation shows that the macroporous framework is composed by the assembly of small interconnected granular particles, leaving small holes in the macropore walls of 300–900 nm thickness. Since no surfactant or template participated in the synthesis, the macroporous structure of titanium dioxide formed spontaneously with the formation mechanism as described previously in the spontaneous template-free assembly of ordered macroporous titania, alumina, aluminosilicate, titanium, and zirconium phosphates [21–26].

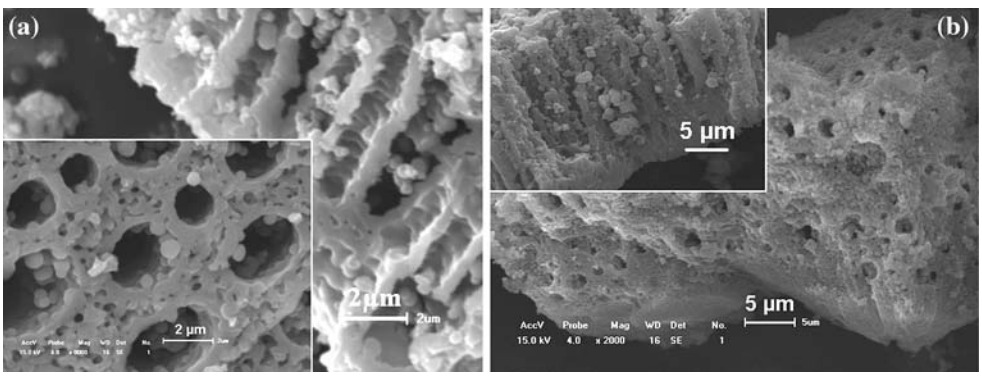

Fig. 3 SEM images of **a** as-synthesized MMTD and **b** 400 °C-calcined 8%-CuO/MMTD catalyst

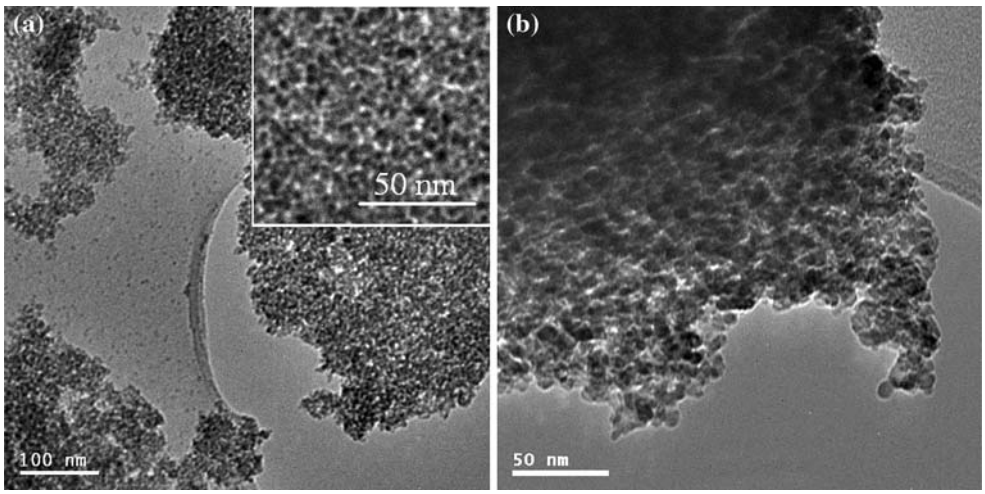

Fig. 4 TEM images of **a** MMTD support and **b** 8%-CuO/MMTD catalyst calcined at 400 °C

Figure 3b shows the SEM images of the 400 °C-calcined 8%-CuO/MMTD catalyst, which is taken as being representative. It is seen that the channel-like macroporous structure can be preserved after the CuO loading and high-temperature calcination. Almost no evident shrinkage of macropore sizes are observed in the supported CuO catalysts. However, the small holes in the macroporous walls of MMTD have partially disappeared because of the possible sintering and solidification of the inorganic framework during the high-temperature calcination.

Transmission electron microscopy (TEM) observations were performed to confirm the fine particulate morphology between the macrochannels of both as-synthesized MMTD and CuO/MMTD catalyst. Figure 4a is the TEM images of the as-synthesized MMTD, demonstrating that the macropore walls have a disordered wormhole-like mesopore structure, formed by the agglomeration of the uniform nanoparticles around 6 nm in size. The accessible pores are connected randomly, lacking discernible long-range order in the pore arrangement among the small particles. Figure 4b is the image of the 400 °C-calcined 8%-CuO/MMTD catalyst, also revealing the wormhole-like mesopores in the macroporous frameworks resulting from the nanoparticle assembly. The nanoparticles are still uniform, but their sizes are a little bigger (around 8 nm), compared with the MMTD sample. The results are consistent with the crystallite sizes obtained by XRD analysis.

N_2 adsorption analysis

Nitrogen adsorption–desorption isotherms and the corresponding pore-size distributions of the as-synthesized and 400 °C-calcined MMTD samples and the CuO/MMTD catalysts with different CuO loading amounts and calcined at different temperatures are shown in Figs. 5 and 6; their

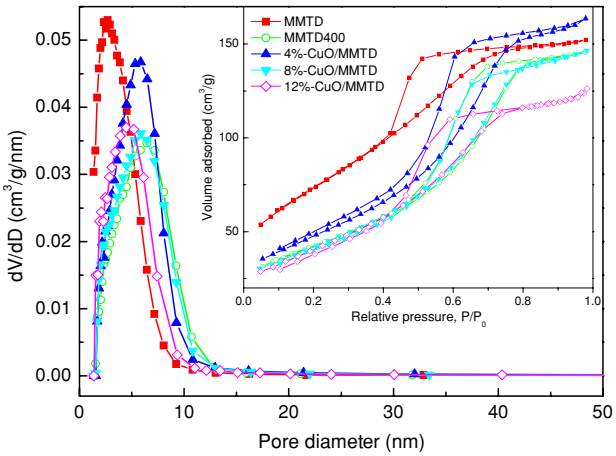

Fig. 5 Pore-size distribution curves and the N_2 sorption–desorption isotherms (inset) of MMTD and CuO/MMTD catalysts with different CuO loading amounts

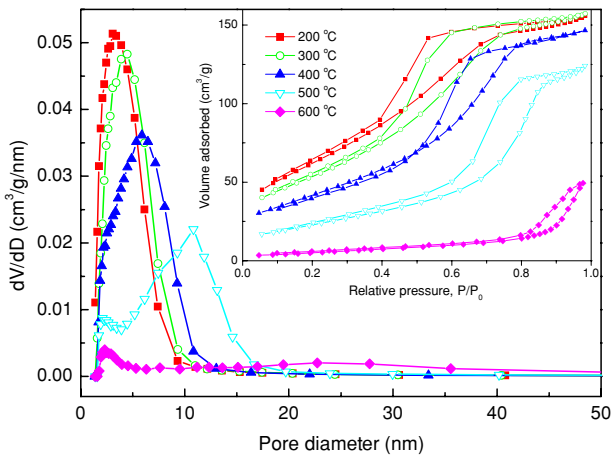

Fig. 6 Pore-size distribution curves and the N_2 sorption–desorption isotherms (inset) of the 8%-CuO/MMTD catalysts calcined at different temperatures

textual properties are also listed in Table 1. All the isotherms are of type IV, characteristic of mesoporous materials, according to the IUPAC classification. A hysteresis loop with a triangular shape and a steep desorption branch is observed in the isotherms, which belongs to the type H2 hysteresis loop, suggesting the presence of pores with narrow mouths and wider bodies (ink-bottle-like pores) [27]. The adsorption isotherm of the as-synthesized MMTD exhibits a large increase in the P/P_0 range of 0.2–0.4 (Fig. 5), which is characteristic of capillary condensation within mesopores. Correspondingly, the pore size of the as-synthesized MMTD is centered at 2.6 nm with a BET surface area of 266 m^2/g. This mesoporosity should be due to the organized aggregation of titania nanoparticles arranged in a fairly uniform way that hydrolysis product of titanium *n*-alkoxide. After calcination, the position of the inflection point in the isotherm of as-synthesized MMTD moved to higher P/P_0 range of 0.4–0.6, indicating the enlargement of the pore size, which is possibly due to the sintering effect. The surface area of the calcined MMTD decreased to 154 m^2/g with pore size of 6.4 nm and pore volume of 0.225 cm^3/g.

As shown in Fig. 5 and Table 1, the pore-size distributions of the 400 °C-calcined *x*%-CuO/MMTD catalysts increase slightly from 5.6 to 5.9 nm with the increase of the CuO loading amount from 4% to 10%, but all of them are smaller than that of 400 °C-calcined MMTD (6.4 nm). However, the pore size of the 12%-CuO/MMTD catalyst is down to 4.6 nm, but is larger than that of the as-synthesized MMTD, since the 12%-CuO/MMTD was calcined at 400 °C. The surface areas of the CuO/MMTD catalysts decreased from 181 to 154 m^2/g with the increase of the CuO loading amount from 4 to 12 wt%, though they are equal or higher than that of 400 °C-calcined MMTD. The pore volumes decreased from 0.266 to 0.195 cm^3/g. The pore volumes of the 10% and 12% CuO/MMTD catalysts are lower than that of 400 °C-calcined MMTD. This may be due to the fact that the excessive CuO particles blocked some mesopores of the MMTD support. XRD analysis has revealed the possible interaction between the nanosized CuO particles and the MMTD support, as a result of the restraint of the titania crystallization. The reduced surface area and pore size in 12%-CuO/MMTD should be thus due to the excessive loading amount of CuO, effectively preventing the growth of titania particles during the 400 °C-calcination.

The inflection point in the isotherms of the 8%-CuO/MMTD catalysts shifted to higher P/P_0 range with the increase of the calcination temperatures (Fig. 6), accompanying with the decrease of the uptake amount of nitrogen. In addition, their surface areas decreased gradually while the pore diameters increased (Table 1). When the calcination temperature increased to the range of 500–600 °C, the pore-size distributions of the catalysts showed bimodal structures. It has been revealed by the XRD patterns that the titania particle size enlargement and phase transformation occured under such temperatures, resulting in the collapse of the mesoporous structure. The possible re-assembly of the nanoparticles of titania and CuO with their strong interaction can then be expected, rendering the formation of one narrow pore-size distribution around 2.1–2.3 nm and one broadened and enlarged distribution (10.8–22.7 nm). The surface area of the 600 °C-calcined sample decreases to only 20 m^2/g, due to the sintering effect and the collapse of the mesoporous structure.

XPS and H_2-TPR analysis

In order to illuminate the surface composition of the studied catalysts and to acquire detailed information on the chemical states of the ions, X-ray photoelectron spectroscopy (XPS) was performed. Figure 7a shows the general survey spectrum of the 400 °C-calcined 8%-CuO/MMTD catalyst, revealing that the surface of the catalyst contains Cu, Ti, O, and C elements. The existence of a small amount of carbon element may be caused by the adventitious hydrocarbons from the XPS instrument itself. Figure 7b–d show the high-resolution XPS spectra of Cu 2p, Ti 2p, and O 1s regions. In Fig. 7b, the XPS peak centered at about 952.4 eV corresponds to Cu $2p_{1/2}$, and the peak at 932.5 eV with a shoulder at 934.2 corresponds to Cu $2p_{3/2}$. The presence of the shake-up peak (about 940.7–943.6 eV), higher Cu $2p_{3/2}$ binding energy (about 934.2 eV), and the $Auger_{L3M4,5M4,5}$ peak (can be observed on the general survey Fig. 7a at about 916.8 eV) are characteristic of Cu^{2+} species and specially of CuO [28–30], suggesting that Cu^{2+} species were present at the surface of MMTD support. On the other hand, the presence of the lower Cu $2p_{3/2}$ binding energy (about 932.5 eV) indicates the existence of the reduced copper species, which may result from strong interaction of copper oxides with the MMTD support [31] or the reduction of Cu^{2+} under the procedure of XPS measurement [32]. The Ti 2p spectrum (Fig. 7c) displays the main peaks of Ti $2p_{3/2}$ and Ti $2p_{1/2}$ at the binding energies of 458.5 and 464.3 eV, respectively, indicating that only titanium in the Ti^{4+} oxidation state can be detected on the surface, which is a clear indication for a well-oxidized sample. The O 1s region (Fig. 7d) can be deconvoluted into two peaks at about 529.8 and 531.4 eV, which indicates the existence of two different oxygen species. The position of the primary O 1s feature (ca. 529.8 eV) is assigned to the lattice oxygen associated with metal oxides, and the shoulder at about 531.4 eV is attributed to the chemisorbed oxygen [14, 15]. The XPS analysis also reveals the surface composition of the 8%-CuO/MMTD catalyst as surface atomic ratio Cu/(Cu + Ti)

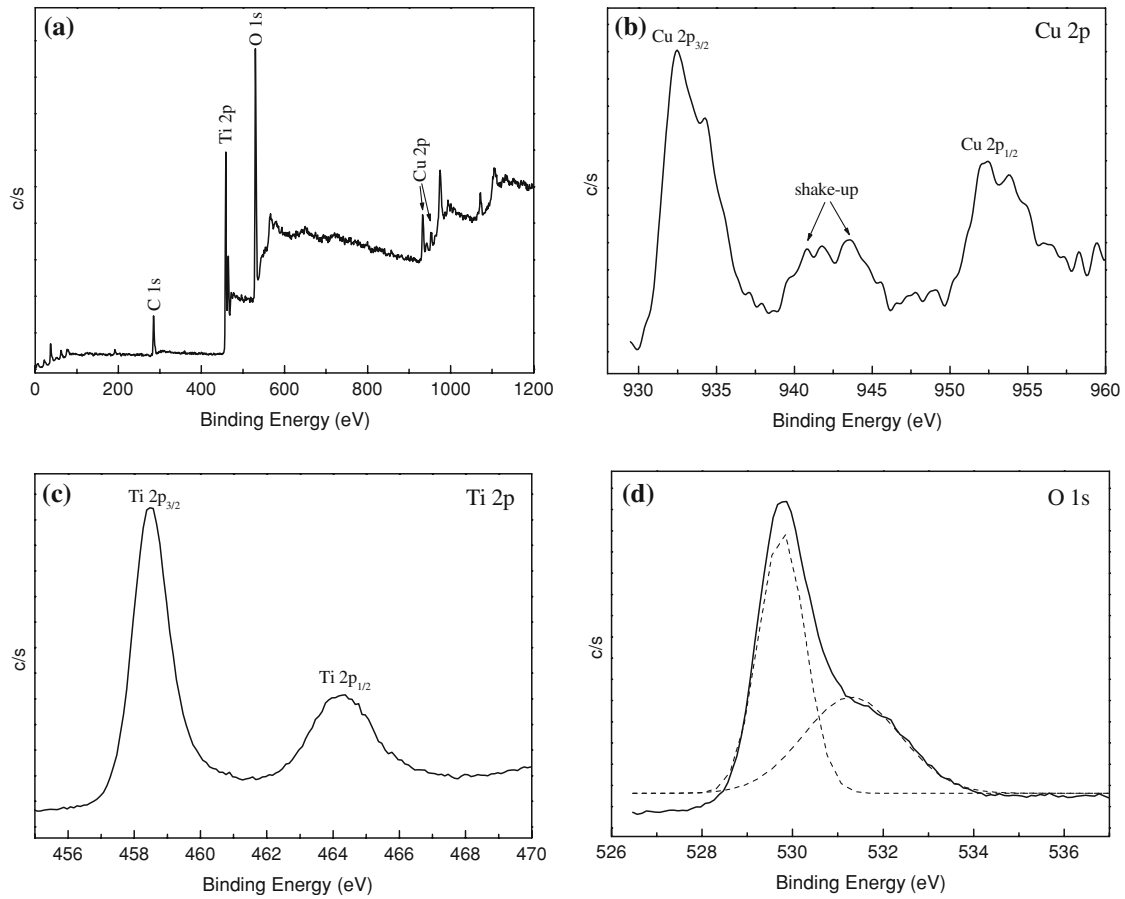

Fig. 7 XPS analysis of 8%-CuO/MMTD catalyst: **a** the general scan, **b** Cu 2p spectrum, **c** Ti 2p spectrum, **d** O 1s spectrum

of 0.195, which is higher than the nominal one (0.08). This indicates a certain surface copper oxide species enrichment, which shows that the CuO particles are really well dispersed on the surface of the MMTD support [28].

H_2-TPR experiments were carried out in order to get information about redox properties of the prepared samples. Figure 8 shows the typical H_2-TPR profile of 8%-CuO/MMTD catalyst calcined at 400 °C, and the reduction profiles of as-synthesized MMTD and pure CuO powder are also presented for comparison. The pure as-synthesized MMTD has two reduction peaks at about 475 and 570 °C, ascribed to the reduction of titania. TPR curve of pure CuO shows a single strong peak of maximum hydrogen consumption at about 363 °C, which is in agreement with the previous report results [4, 6].On the other hand, in the TPR curve of the CuO/MMTD catalyst, besides the reduction peaks of pure titania (475 and 570 °C), four new reduction peaks are observed at about 170, 188, 280, and 400 °C, respectively. The loading of CuO causes the significant effect on the reducibility of meso–macroporous titania. The peak around 400 °C might be the reduction of surface titania species ($Ti^{4+} \rightarrow Ti^{3+}$) on the border with CuO nanoparticles, shifted from higher temperature, suggesting

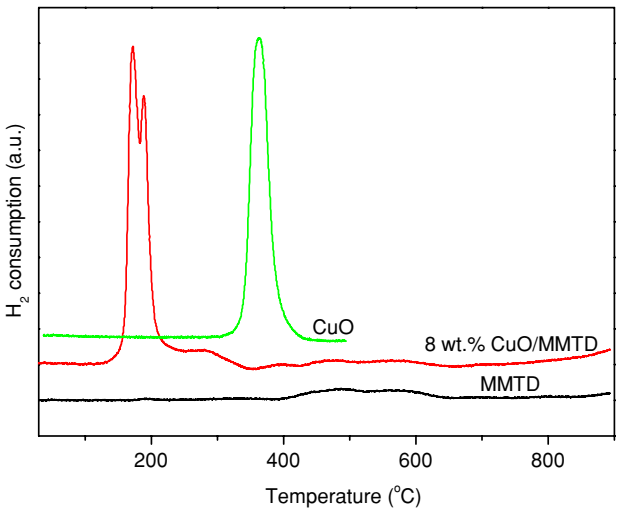

Fig. 8 H_2-TPR profiles of pure CuO, as-synthesized MMTD, and 8%-CuO/MMTD catalyst calcined at 400 °C

the formation of more easily reducible species due to the presence of foreign metal species [33]. The peaks at about 170, 188, and 280 °C are mainly related to the reduction of Cu species due to the much higher reducibility of Cu

species compared with titanium oxides. The reduction temperature of supported copper species lower than that of pure CuO is due to the synergistic effects between CuO and the MMTD support; MMTD is promoting the reduction of CuO. In general,, CuO gets reduced in a wider temperature range by a two-step stage when contacting with CeO_2, SnO_2, $Ce_xZr_{1-x}O_2$, ceria-modified anatase, etc. [4, 11, 12, 32]. The first reduction step is always promoted by the interaction between CuO and the support, while the second step is delayed by the stabilization effect of the support on the cations at the medium valence. The two overlapped low-temperature reduction peaks have been observed in the reported CuO-based catalysts supported on some metal oxides [4, 14, 15, 31], and thus the peaks at 170 and 188 °C in the hierarchical CuO/MMTD catalyst sample can be ascribed to the reduction of highly dispersed CuO species (X-ray amorphous form), strongly interacting with the support, into Cu^+ and Cu^0, respectively, which are regarded as the active sites for CO oxidation. While the weak shoulder peak around 280 °C may correspond to the reduction of small amount of larger CuO particles (or bulk CuO) on the MMTD surface.

Catalytic activity

The catalytic performance of the hierarchical MMTD-supported CuO catalysts were tested by low-temperature catalytic CO oxidation. Figures 9 and 10 show the variation of catalytic activity of the prepared CuO/MMTD catalysts for low-temperature CO oxidation as a function of reaction temperature. All the catalysts present a similar behavior revealing that the CO oxidation activity increased with the increase of the catalytic reaction temperature. The "light-off" temperatures for 100% CO conversion of the catalysts and the highest conversion of the catalysts which

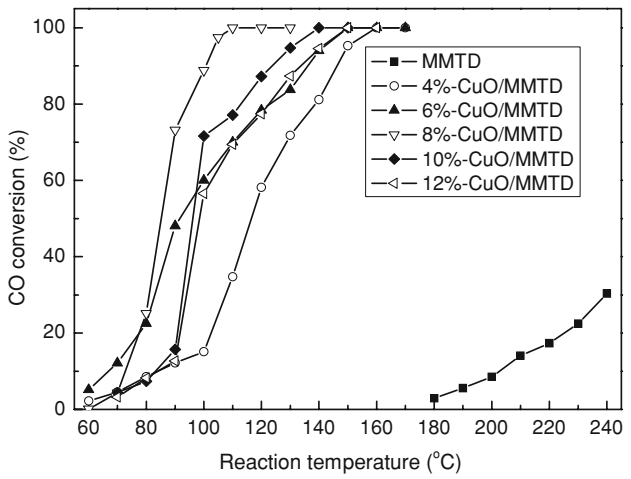

Fig. 9 Catalytic activity for CO oxidation of CuO/MMTD catalysts with different CuO loading amounts calcined at 400 °C

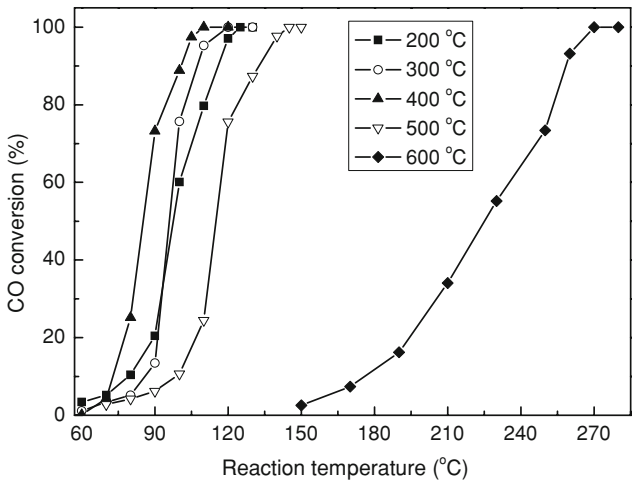

Fig. 10 Catalytic activity for CO oxidation of 8%-CuO/MMTD catalysts calcined at different temperatures

cannot reach 100% conversion in the present reaction condition are shown in Table 1.

Figure 9 presents the catalytic activity of CuO/MMTD catalysts with different loading amounts of CuO calcined at 400 °C, together with the catalytic activity of pure MMTD for comparison purpose. It is noted from Fig. 9 that the observed activity of the pure MMTD support in CO oxidation is quite low, while the addition of CuO significantly increases the catalytic activity of all the samples. The 400 °C-calcined pure CuO had almost no activity under the present measuring condition in the reaction temperature range of 60–250 °C, and the observable CO-conversion appeared only at the reaction temperature above 250 °C. This illustraates that there is a synergistic effect between CuO and MMTD support, which strongly affects the catalytic activity of the CuO/MMTD catalysts in low-temperature CO oxidation. In all the CuO/MMTD catalysts with the CuO loading amounts ranging from 4 to 12 wt%, the 8%-CuO/MMTD catalyst exhibited the highest activity with CO total conversion at 110 °C. This indicates that the finely dispersed CuO species should be responsible for the activity, as confirmed by the H_2-TPR and XRD results. Liu and Flytzani-Stephanopoulos [34] suggested that the activity of catalyst derived primarily from the combination of finely dispersed copper-support systems, and bulk CuO had negligible contributions. Our previous investigation [14] of mesoporous $Ce_{0.8}Zr_{0.2}O_2$-supported CuO catalysts provided the similar results. Therefore, when the loading amount of CuO was high, the excess CuO species would not only cover some of the active sites, but also lead to the growth of CuO particles or bulk CuO formation, which have negative effect on the catalytic activity of low-temperature CO oxidation.

The influence of the precalcination temperature on the catalytic activity of the CuO/MMTD catalysts in CO

oxidation was presented in Fig. 10. It is seen that the catalytic activity of the 8%-CuO/MMTD catalysts increased with the precalcination temperature from 200 to 400 °C, but decreased from 400 to 600 °C. The 400 °C-calcined 8%-CuO/MMTD catalyst exhibited the highest catalytic activity on CO oxidation with CO total conversion at 110 °C, while the total CO conversion temperature over the 600 °C-calcined one was 270 °C. The XRD and N_2adsorption analysis has revealed that the heat treatment made the decrease of the surface areas and the increase of the MMTD particle sizes with the increase of calcination temperatures. In the 600 °C-calcined 8%-CuO/MMTD catalyst, the rutile phase appeared with the collapse of the mesoporous structure, and the surface area is the lowest with 20 m^2/g and the largest particle's size is 28.7 nm. Thus, the observed difference in the catalytic activities of the CuO/MMTD catalysts calcined at different temperature maybe due to the agglomeration of the catalysts, the decrease of the surface area, and the increase of particle sizes by the increase of the calcination temperature. The observed high activity of these CuO/MMTD catalysts should benefit from their high surface area and large mesoporosity.

In order to highlight the advantage of the hierarchical meso–macroporous structure of the CuO/MMTD nanocatalyst, the commercially available TiO_2 powder with particle diameter of 100 nm and surface area of 10 m^2/g, and mesoporous titania without macrochannels (MP-TiO_2) prepared by nonionic surfactant templating under vigorous stirring [33] were used as supports of CuO catalysts (same CuO loading amount of 8 wt% and after 400 °C-calcination) by the same manner as the preparation of CuO/MMTD catalyst. The surface area of the obtained 8%-CuO/MP-TiO_2 is 130 m^2/g with the mesopore size of 8 nm, which is comparable with that of 8%-CuO/MMTD. The comparative study of the catalytic activity of these three catalysts was presented in Fig. 11. It is seen clearly from Fig. 11 that the CO total conversion temperatures on the CuO/MP-TiO_2 and CuO/commercial-TiO_2 powder catalysts are 120 and 150 °C, respectively, which are higher than that of CuO/MMTD (110 °C). This indicates that the supported CuO catalysts with high catalytic activity can be obtained by using hierarchically mesoporous–macroporous titania as support. Compared with CuO/commercial-TiO_2 that is a nonporous catalyst with low surface area, both CuO/MP-TiO_2 and CuO/MMTD possess mesoporous frameworks that provide a large surface-to-volume ratio, and hence more active sites are available for CO oxidation [19]. The macrochannels in the CuO/MMTD can render the faster diffusion of the reactant and product molecules, resulting in the higher CO conversion rate than that obtained in the CuO/MP-TiO_2 catalyst without macrochannels. The poor activity of CuO/commercial-TiO_2 can thus be explained by its structural and chemical properties, e.g., low-surface-area and nonporosity. It has been revealed that the dispersion states of CuO particles can be finer with the smaller CuO crystallites for the higher-surface-area catalysts [35], and more exposed active sites formed with higher catalytic activity on the high-surface-area catalysts than on the low-surface-area ones. Macropores permit facile transport of gas molecules in catalysts, and the mesoporous structure favors specific surface area for large active sites, beneficial to the enhanced catalytic activity.

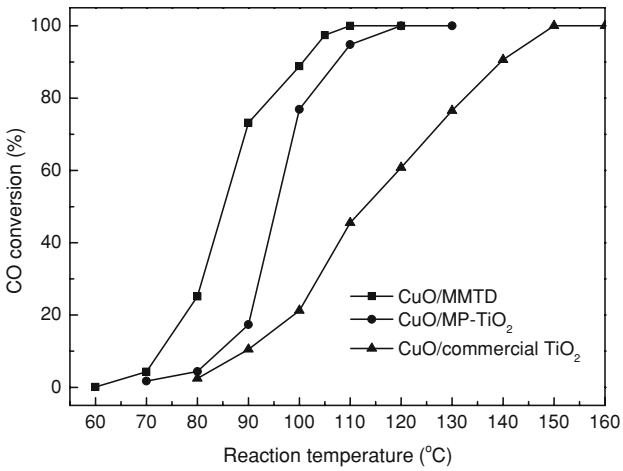

Fig. 11 Catalytic activity for CO oxidation of MMTD, MP-TiO_2, and commercial TiO_2-supported 8%-CuO catalysts calcined at 400 °C

Conclusions

Hierarchically meso–macroporous titania was prepared by a simple surfactant-free process, and its use as support of CuO nanocatalysts was demonstrated. The hierarchical meso–macroporous networks are preserved in the resultant 400 °C-calcined CuO/MMTD catalysts with high surface areas, indicating the structural stability of the catalysts, which are active in the low-temperature CO oxidation. The XPS and H_2-TPR analysis indicated that CuO species were highly dispersed on the catalyst surfaces. The influence of the loading amount of CuO and precalcination temperature on the catalytic properties of the catalysts was investigated. The CuO/MMTD catalyst with 8 wt% CuO loadings and calcined at 400 °C has the highest catalytic activity. Moreover, the catalytic activity of CuO/MMTD catalyst is higher than that of the commercially available TiO_2 powder-supported and mesoporous titania-supported CuO catalysts with the same CuO loading amount, indicating the beneficial effect of the hierarchical meso–macroporous structure. The synergistic effect between CuO and the MMTD support, the highly dispersed CuO nanoparticles, the mesoporous–macroporous framework, the high surface

area, and the uniform distribution of nanoscale particle size were responsible for the high catalytic activity of the CuO/MMTD nanocatalysts for low-temperature CO oxidation.

Acknowledgements This study was supported by the National Natural Science Foundation of China (Nos. 20473041 and 20673060), the National Basic Research Program of China (No. 2009CB623502), the Specialized Research Fund for the Doctoral Program of Higher Education (20070055014), the Natural Science Foundation of Tianjin (08JCZDJC21500), the Fund from Hebei Provincial Department of Education (2007313), the Chinese-Bulgarian Scientific and Technological Cooperation Project, the Program for New Century Excellent Talents in University (NCET-06-0215), and Nankai University.

References

1. Haruta M, Tsubota S, Kobayashi T, Kageyama H, Genet MJ, Delmon B (1993) J Catal 144:175
2. Schryer DR, Upchur BT, Sidney BD, Brown KG, Hoflund GB, Herz RK (1991) J Catal 130:314
3. Engel T, Ertl G (1979) Adv Catal 28:1
4. Luo MF, Zhong YJ, Yuan XX, Zheng XM (1997) Appl Catal A 162:121
5. Tang X, Zhang B, Li Y, Xu Y, Xin Q, Shen W (2005) Appl Catal A 288:116
6. Lin R, Luo MF, Zhong YJ, Yan ZL, Liu GY, Liu WP (2003) Appl Catal A 255:331
7. Tsodikov MV, Trusova YeA, Slivinski YeV, Hernandez GG, Kochubey DI, Lipovich VG, Navio JA (1998) Stud Surf Sci Catal 118:679
8. Huang J, Wang S, Zhao Y, Wang X, Wang S, Wu S, Zhang S, Huang W (2006) Catal Commun 7:1029
9. El-Shobaky GA, Fagal GA, Mokhtar M (1997) Appl Catal A 155:167
10. Wan H, Wang Z, Zhu J, Li X, Liu B, Gao F, Dong L, Chen Y (2008) Appl Catal B 79:254
11. Wang SP, Wang XY, Huang J, Zhang SM, Wang SR, Wu SH (2007) Catal Commun 8:231
12. Zhang TY, Wang SP, Yu Y, Su Y, Guo XZ, Wang SR, Zhang SM, Wu SH (2008) Catal Commun 9:1259
13. Cheng T, Fang Z, Hu Q, Han K, Yang X, Zhang Y (2007) Catal Commun 8:1167
14. Cao J-L, Wang Y, Zhang T-Y, Wu S-H, Yuan Z-Y (2008) Appl Catal B 78:120
15. Cao J-L, Wang Y, Yu X-L, Wang S-R, Wu S-H, Yuan Z-Y (2008) Appl Catal B 79:26
16. Yuan ZY, Su BL (2006) J Mater Chem 16:663
17. Blin JL, Leonard A, Yuan ZY, Gigot L, Vantomme A, Cheetham AK, Su BL (2003) Angew Chem Int Ed 42:2872
18. Tidahy HL, Siffert S, Lamonier J-F, Zhilinskaya EA, Aboukaïs A, Yuan Z-Y, Vantomme A, Su B-L, Canet X, De Weireld G, Frère M, N'Guyen TB, Giraudon J-M, Leclercq G (2006) Appl Catal A 310:61
19. Ho C, Yu JC, Wang X, Lai S, Qiu Y (2005) J Mater Chem 15:2193
20. Idakiev V, Tabakova T, Naydenov A, Yuan Z-Y, Su B-L (2006) Appl Catal B 63:178
21. Collins A, Carriazo D, Davis SA, Mann S (2004) Chem Commun 5:568
22. Ren TZ, Yuan ZY, Su BL (2004) Chem Commun 23:2730
23. Deng W, Shanks BH (2005) Chem Mater 17:3092
24. Yuan ZY, Ren TZ, Azioune A, Pireaux JJ, Su BL (2006) Chem Mater 18:1753
25. Ren TZ, Yuan ZY, Azioune A, Pireaux JJ, Su BL (2006) Langmuir 22:3886
26. Yu JG, Su YR, Cheng B (2007) Adv Funct Mater 17:1984
27. Kruk M, Jaroniec M (2001) Chem Mater 13:3169
28. Avgouropoulos G, Ioannides T (2003) Appl Catal A 244:155
29. Bechara R, Aboukaïs A, Guelton M, D'Huysser A, Grimblot J, Bonnelle JP (1990) Spectrosc Lett 23:1237
30. Cousin R, Abi-Aad E, Capelle S, Courcot D, Lamonier J-F, Aboukaïs A (2007) J Mater Sci 42:6188. doi:10.1007/s10853-006-1165-6
31. Kundakovic Lj, Flytzani-Stephanopoulos M (1998) Appl Catal A 171:13
32. Zhu HY, Shen MM, Kong Y, Hong JM, Hu YH, Liu TD, Dong L, Chen Y, Jian C, Liu Z (2004) J Mol Catal A 219:155
33. Idakiev V, Tabakova T, Yuan Z-Y, Su B-L (2004) Appl Catal A 270:135
34. Liu W, Flytzani-Stephanopolos M (1996) Chem Eng J 64:293
35. Luo MF, Ma JM, Lu JQ, Song YP, Wang YJ (2007) J Catal 246:52